Lifetime measurement for the 2_1^+ state in ^{140}Sm and the onset of collectivity in neutron-deficient Sm isotopes

F. L. Bello Garrote,[1] A. Görgen,[1] J. Mierzejewski,[2] C. Mihai,[3] J. P. Delaroche,[4] M. Girod,[4] J. Libert,[4] E. Sahin,[1] J. Srebrny,[2] T. Abraham,[2] T. K. Eriksen,[1] F. Giacoppo,[1] T. W. Hagen,[1] M. Kisielinski,[2] M. Klintefjord,[1] M. Komorowska,[2] M. Kowalczyk,[2] A. C. Larsen,[1] T. Marchlewski,[2] I. O. Mitu,[3] S. Pascu,[3] S. Siem,[1] A. Stolarz,[2] and T. G. Tornyi[1,5]

[1]*Department of Physics, University of Oslo, N-0316 Oslo, Norway*

[2]*Heavy Ion Laboratory, University of Warsaw, PL-02-093 Warsaw, Poland*

[3]*Horia Hulubei National Institute of Physics and Nuclear Engineering, R-077125 Bucharest, Romania*

[4]*CEA, DAM, DIF, F-91297 Arpajon, France*

[5]*Institute of Nuclear Research of the Hungarian Academy of Sciences (MTA ATOMKI), H-4001 Debrecen, Hungary*

(Received 19 June 2015; revised manuscript received 3 August 2015; published 21 August 2015)

Background: The chain of Sm isotopes exhibits a wide range of nuclear shapes and collective behavior. While the onset of deformation for $N > 82$ has been well studied both experimentally and theoretically, fundamental data is lacking for some Sm isotopes with $N < 82$.

Purpose: Electromagnetic transition rates represent a sensitive test of theoretical nuclear structure models. Lifetime measurements are furthermore complementary to Coulomb excitation experiments, and the two methods together can give access to spectroscopic quadrupole moments.

Method: The lifetime of the 2_1^+ state in ^{140}Sm was measured with the recoil-distance Doppler shift technique using the reaction ^{124}Te(^{20}Ne, 4n)^{140}Sm at 82 MeV. Theoretical calculations were performed based on a mapped collective Hamiltonian in five quadrupole coordinates (5DCH) and the Gogny D1S interaction.

Results: The lifetime of the 2_1^+ state in ^{140}Sm was found to be 9.1(6) ps, corresponding to a $B(E2; 2_1^+ \rightarrow 0_1^+)$ value of 51(4) Weisskopf units. The theoretical calculations are in very good agreement with the experimental result.

Conclusions: The $B(E2; 2_1^+ \rightarrow 0_1^+)$ value for ^{140}Sm fits smoothly into the systematic trend for the chain of Sm isotopes. The new beyond-mean field calculations are able to correctly describe the onset of collectivity in the Sm isotopes below the $N = 82$ shell closure for the first time.

DOI: 10.1103/PhysRevC.92.024317 PACS number(s): 21.10.Tg, 21.60.Jz, 23.20.Js, 27.60.+j

I. INTRODUCTION

The chain of Sm isotopes covers a very wide range of nuclear shapes and collective behavior, from spherical shape and noncollective excitations for ^{144}Sm at the $N = 82$ shell closure, to highly rotational nuclei with some of the most deformed ground-state shapes in the nuclear chart, considering both the extremely neutron-deficient and neutron-rich isotopes around ^{132}Sm and ^{160}Sm, respectively [1,2]. The transition from spherical to nearly axially deformed prolate shapes for $N > 82$ has received particular attention from both experimentalists and theorists because of the rapid onset of deformation at $N = 90$, and the presence of octupole correlations near $N = 88$. The abrupt shape transition from $N = 88$ to $N = 90$ is observed also in other isotopic chains near the $Z = 64$ subshell closure, and it was explained by the eradication of the $Z = 64$ subshell gap, and the polarization of the proton core due to the occupation of proton-neutron spin-orbit partner orbitals when the neutron number reaches $N = 90$ [3]. The ^{152}Sm nucleus is considered a good realization of the so-called X(5) critical point symmetry, which analytically describes a first-order phase transition from spherical, vibrational to well-deformed, rotational nuclei [4,5]. The shape transition near ^{152}Sm was also studied with various microscopic approaches, using, e.g., relativistic [6], Skyrme [7], or Gogny [8,9] energy density functionals. In addition to the onset of quadrupole deformation, there is experimental evidence for octupole correlations in ^{148}Sm [10] and ^{150}Sm [11,12]. A recent spectroscopic study found evidence for octupole excitations built both on the 0_1^+ and 0_2^+ states in ^{152}Sm, which led to the interpretation that ^{152}Sm exhibits features of shape coexistence rather than critical-point symmetry [13].

By comparison, the onset of collectivity for neutron-deficient Sm isotopes with $N < 82$ is somewhat poorly studied and lacking fundamental experimental data. The observation of low-lying γ bands in ^{136}Sm and ^{140}Sm [14] and ^{138}Sm [15] was interpreted as from a triaxial deformation present in these nuclei, supported by triaxial-rotor calculations based on a Woods-Saxon potential [14]. However, the spins of the 2^+ and 3^+ members of the presumed γ band in ^{140}Sm were revised in a subsequent experiment studying the β decay of ^{140}Eu [16]. Relativistic Hartree-Fock-Bogoliubov calculations with a separable pairing force describe the ground-state shapes of even-even Sm isotopes with $N < 80$ as γ soft, where the overall deformation increases with decreasing neutron number and the equilibrium shape changes from slightly oblate in ^{140}Sm to prolate in the lighter isotopes [17]. Earlier relativistic mean-field calculations, which were restricted to axial deformations, also predicted oblate ground-state shapes for the $N = 78$ isotones ^{138}Nd, ^{140}Sm, ^{142}Gd, and ^{144}Dy, with prolate deformation developing rapidly for the lighter nuclei with $N \leqslant 76$ [18]. Hartree-Fock-Bogoliubov calculations based on the Gogny force also predict a smooth onset of deformation with decreasing neutron number below $N = 82$, and a transition from prolate ground-state shapes for the $N = 78$ isotones with $Z \leqslant 62$ to oblate for $Z \geqslant 64$ [9]. An analysis of the low-lying states in neutron-deficient

 ©2015 American Physical Society

Sm isotopes using the interacting boson approximation (IBA) yielded parameters that place ^{140}Sm along the U(5)-O(6) leg of the IBA symmetry triangle, i.e., with collective properties in between a spherical vibrator and a γ-soft vibrator, whereas the lighter isotopes become more and more consistent with axial rotors [19]. The apparent γ softness of the neutron-deficient Sm isotopes suggests that the transition from a spherical shape to an axially symmetric prolate shape is different for the isotopes with $N < 82$ compared to those with $N > 82$. Experimental information on the nucleus ^{140}Sm can help to understand the onset of deformation and evolution of the nuclear shape in the Sm isotopes with $N < 82$.

The quasirotational ground-state band of ^{140}Sm was first observed following α-induced reactions [20]. The structure of ^{140}Sm above 3 MeV excitation energy is dominated by the occurrence of two 10^+ isomers: the $(\nu h_{11/2})^{-2}$ state at 3172 keV with 19.4(7) ns half-life and the $(\pi h_{11/2})^2$ state at 3211 keV with 5.20(14) ns half-life [21]. The neutron-hole and proton-particle character of the two isomers was confirmed by g-factor measurements [22]. An analysis of the $B(M1)$ strength of the transition connecting the two isomeric states suggested that there is practically no mixing between the proton and neutron configurations of the isomers, which is consistent with their almost degenerate energy [22]. The absolute quadrupole moment of the $(\nu h_{11/2})^{-2}$ isomer was measured be $|Q| = 167(48)$ fm^2 using angular distribution techniques in an electric field gradient, corresponding to a quadrupole deformation parameter of $|\beta| = 0.12(4)$ [23]. The rotational bands observed on top of the 10^+ isomers with proton-particle and neutron-hole character are very similar to the ground-state bands in ^{138}Nd and ^{142}Sm, respectively [21]. The level scheme of ^{140}Sm was afterwards extended to higher spins and excitation energies and explained by couplings of proton particles and neutron holes to the respective core nuclei [24]. The early studies interpreted the $(\pi h_{11/2})^2$ state as oblate and the $(\nu h_{11/2})^{-2}$ state as prolate, based on the argument that aligned particles induce oblate and aligned holes prolate deformation [21,23]. A subsequent experiment yielded lifetimes of states in the rotation-aligned bands above the 10^+ isomers, and it was argued that proton excitations involving low-Ω orbitals at the bottom of the $h_{11/2}$ shell require prolate deformation, whereas neutron excitations involving low-Ω orbitals at the top of the $h_{11/2}$ shell require oblate shape [25].

While there is firm evidence for shape coexistence in ^{140}Sm above 3 MeV excitation energy, the shape and collectivity of the states at lower energy is less clear. A surprisingly low-lying 0_2^+ state was reported at an excitation energy of only 990 keV [16], which could potentially hint to shape coexistence also near the ground state. However, a recent measurement of γ-γ angular correlations suggests that the original spin assignment of $I^\pi = 2^+$ for the state at 990 keV and the interpretation as the head of a γ-vibrational band is correct after all [26,27]. Because of the long lifetime of the 10^+ states it is difficult to measure the much shorter lifetimes of the states below with Doppler-shift methods. The 10^+ isomers are bypassed by a negative-parity band [24]. However, the 7^- state is expected to be based on the $\nu(h_{11/2}^{-1} \otimes d_{3/2}^{-1})$ configuration and systematics suggests that its lifetime is of the order of 150 ps [28], preventing prompt feeding of the 2^+ and 4^+ states of the ground-state band. Consequently, no $B(E2)$ values between states of the ground-state band are known below the 10^+ isomers. The lack of electric quadrupole transition probabilities for ^{140}Sm makes it difficult to investigate the onset of collectivity for the Sm isotopes for $N < 82$ and compare it to the isotopes with $N > 82$, where $B(E2)$ values are known [29].

The results of a new lifetime measurement for the 2_1^+ state in ^{140}Sm using the recoil-distance Doppler shift (RDDS) technique [30] are presented in this article. The resulting $B(E2; 2_1^+ \rightarrow 0_1^+)$ value extends the systematics towards the $N = 82$ shell closure and contributes to the understanding of how quadrupole collectivity evolves in this mass region. The lifetime measurement is complementary to a recent Coulomb excitation experiment with a radioactive ^{140}Sm beam [26,31]. A precise measurement of the lifetime of the 2_1^+ state can be used to constrain the Coulomb excitation analysis, as the Coulomb excitation probability for the 2_1^+ state depends both on the $B(E2; 0_1^+ \rightarrow 2_1^+)$ transition strength and the spectroscopic quadrupole moment $Q_s(2_1^+)$. Knowing the $B(E2)$ transition probability from an independent measurement enhances the sensitivity to the reorientation effect and allows a more precise measurement of the spectroscopic quadrupole moment [32].

The article is organized as follows: The experimental procedure is described in Sec. II; the results of the experiment are presented in Sec. III together with details of the data analysis; the results are discussed and compared with various theoretical models in Sec. IV, before a summary and conclusions are given in Sec. V.

II. EXPERIMENTAL DETAILS

The main difficulty in measuring lifetimes of states in the ground-state band of ^{140}Sm is related to the fact that prompt feeding paths are blocked by the long-lived 10^+ isomers and the 7^- state. The entire γ-ray flux from high-spin states seems to pass through either one of them, and there is no indication of a decay path that bypasses any of these states [24]. Under these circumstances, lifetimes of the states below the isomers can only be measured using the RDDS technique, if a reaction can be found which results in sufficiently strong prompt feeding of the states, and if these prompt feeding paths are selected by applying γ-γ coincidence gates. A previous RDDS measurement used the reaction ^{106}Pd(^{37}Cl, p2n)^{140}Sm at a beam energy of 143 MeV and an array consisting of three Compton-suppressed Ge detectors and a BaF_2 multiplicity filter [25]. The reaction parameters were optimized for the population of high-spin states, and the efficiency of the Ge detectors was insufficient for the detection of γ-γ coincidences. Consequently, it was only possible to measure lifetimes of states above the 10^+ isomers, but not below [25].

A new experiment to measure lifetimes below the isomers was performed at the Heavy Ion Laboratory of the University of Warsaw. The strategy of the new experiment was to use a relatively light projectile and a beam energy just above the Coulomb barrier to limit the population of high-spin states and maximize the direct population of states with spin $I < 10$. The experiment used the reaction ^{124}Te(^{20}Ne, 4n)^{140}Sm with

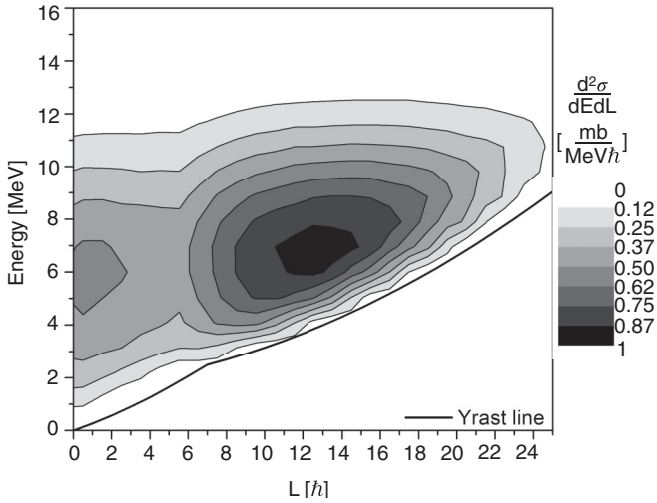

FIG. 1. Entry-state distribution for the reaction ^{124}Te(^{20}Ne, 4n)^{140}Sm at a projectile energy of 82 MeV calculated with the code COMPA [34].

a projectile energy of 82 MeV in the center of the target, which is very close to the Coulomb barrier. The reaction was chosen based on cross-section calculations performed with the codes PACE [33] and COMPA [34]. Figure 1 shows the entry-state distribution calculated with COMPA for the chosen reaction after the evaporation of four neutrons. The calculations suggest that the maximum of the spin distribution is at spin $I \approx 13$, but that a significant fraction of the cross section populates low-spin states with $I < 10$.

Lifetimes were measured using the RDDS technique with the Köln-Bucharest Plunger device coupled to the EAGLE spectrometer [35]. Because of the difficulty of making a stretchable self-supporting tellurium target, a 0.7 mg/cm^2-thick ^{124}Te layer was evaporated in high vacuum onto a 5 mg/cm^2-thick gold foil which was cooled during the vapor deposition. The ^{20}Ne beam was accelerated with the U200P cyclotron of the Heavy Ion Laboratory to an energy of 95 MeV. During the experiment, the gold backing of the target was facing the beam. The energy loss of the beam in the backing was approximately 13 MeV, resulting in the desired projectile energy of 82 MeV in the center of the ^{124}Te layer. The recoils exiting the target were stopped after a variable flight path with a gold stopper foil of 5 mg/cm^2 thickness. Both the target and the stopper foils were stretched to obtain smooth and even surfaces. Measurements were taken for nine different distances between the target and stopper ranging from 14 to 120 μm. The average measuring time for each distance was 18 h. During this time the distance was kept constant using a feedback mechanism based on measuring the capacitance between the two foils.

The EAGLE array consisted of 12 Compton-suppressed HPGe detectors with 70% relative efficiency at 1.3 MeV. Four of them were mounted at 37°, three at 79°, and five at 143° with respect to the beam direction. Only the detectors at 37° (forward) and 143° (backward) were able to cleanly resolve the Doppler-shifted and stopped components of the $2_1^+ \rightarrow 0_1^+$ transition.

III. DATA ANALYSIS AND RESULTS

For each distance the recorded data was sorted into three separate γ-γ coincidence matrices for coincidences between two forward detectors, two backward detectors, or between one forward and one backward detector, respectively. The backward detectors suffered from background originating from a beam collimator located just upstream from the detector array. Because of their comparatively poor quality the backward-backward coincidence matrices were discarded from further analyses.

The main challenge of the experiment was to select events in which low-lying states were promptly fed without passing through the isomeric states. Prompt feeding of the 2_1^+ state can be assured by gating on the Doppler-shifted component of the $4_1^+ \rightarrow 2_1^+$ transition. The selection of prompt feeding of the 2_1^+ state is illustrated in Fig. 2. The top panel shows a section of the total projection of the forward-forward matrix at a target-stopper distance of 40 μm, which is a very sensitive distance to determine the lifetime of the 2_1^+ state. Both the $2_1^+ \rightarrow 0_1^+$ transition at 531 keV and the $4_1^+ \rightarrow 2_1^+$ transition at 715 keV can be seen in the spectrum, together with peaks from the Coulomb excitation of gold and transitions originating from ^{141}Sm, which were populated through the ^{124}Te(^{20}Ne,3n) reaction. Although most of the γ rays detected from the $2_1^+ \rightarrow 0_1^+$ and the $4_1^+ \rightarrow 2_1^+$ transitions were emitted after reaching the stopper foil and are consequently unshifted in energy due to delayed feeding from the isomers, small shifted components can be seen for both transitions. It was not possible to determine whether the prompt feeding is due to a weak decay path of discrete transitions that are bypassing the isomers, or due to direct feeding of the low-lying states by statistical transitions from the continuum. The presence of the weak prompt feeding component allows gating on the shifted component of the $4_1^+ \rightarrow 2_1^+$ transition to extract the lifetime of the 2_1^+ state. However, the statistics of the gated spectra is somewhat low, and special care has to be taken to subtract the background from Compton scattering events underlying the shifted component of the $4_1^+ \rightarrow 2_1^+$ transition. A wide background region was selected on both sides of the 715-keV peak as shown in Fig. 2(a), and a normalized fraction of the background-gated spectrum was subtracted from the spectrum gated on the shifted component of the $4_1^+ \rightarrow 2_1^+$ transition. It was verified that none of the small peaks that are visible in the selected background region are in coincidence with the $2_1^+ \rightarrow 0_1^+$ transition. As can be seen in Fig. 2, the intensity ratio between the shifted and unshifted components of the $2_1^+ \rightarrow 0_1^+$ transition changes significantly after background subtraction. This happens because the unshifted component of the 531-keV line is much stronger than the shifted one, and Compton events are mostly in coincidence with the stopped component of the $2_1^+ \rightarrow 0_1^+$ transition.

The same procedure was applied to all spectra recorded at the various distances between the target and stopper foils. Background-subtracted coincidence spectra gated on γ rays detected at 143° from the backward-forward matrices were added to those gated on γ rays detected at 37° from the forward-forward matrices to result in the final set of spectra which was used to determine the lifetime of the 2_1^+ state.

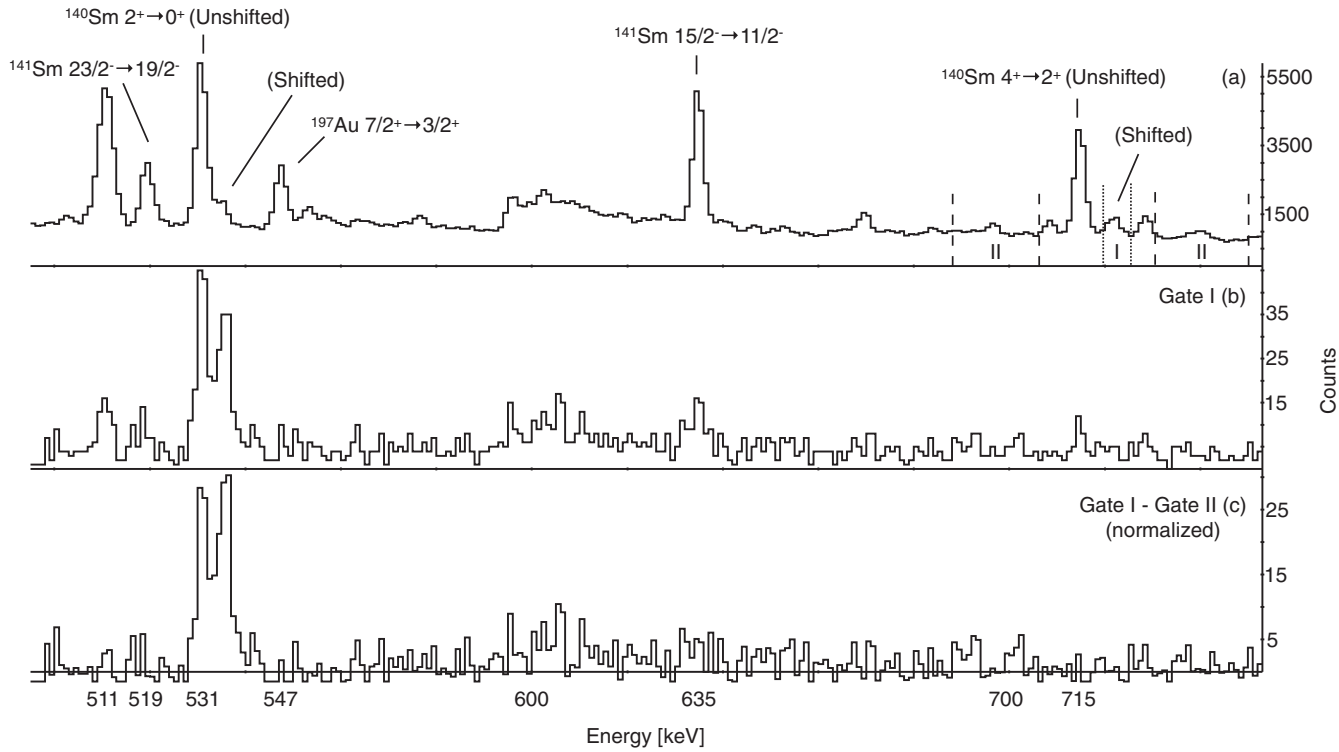

FIG. 2. Projections of the forward-forward matrix for a distance of 40 μm between the target and stopper foils. The top panel (a) shows a section of the total projection. The same section is shown in the middle panel (b) after applying a coincidence gate on the shifted component of the $4_1^+ \rightarrow 2_1^+$ transition. The bottom panel (c) shows the same coincidence spectrum after the normalized subtraction of background gates as marked in the top panel.

The Doppler-shifted and stopped components of the $2_1^+ \rightarrow 0_1^+$ transition in the background-subtracted spectra observed under forward angles and gated on the shifted component of the $4_1^+ \rightarrow 2_1^+$ transition are shown in Fig. 3 for the nine different distances. The intensities of the two components were determined by fitting two Gaussians. In case of peaks with low intensity the width of the Gaussian was fixed to the value that was determined from the spectra taken at the shortest and longest distance where the respective components are strongest. The average energy of the shifted component was found to be 535.5(3) keV. From the energy difference between the two peaks the average recoil velocity was determined to be $v/c = 1.15(1)\%$. This value is consistent with the average recoil velocity calculated from the reaction kinematics taking into account the energy loss of the beam and recoils in the target.

The intensities of the shifted and unshifted components have to be normalized to account for differences in beam intensity and measuring time for the different target-stopper distances. The normalization factor was chosen as the total area of the $2_1^+ \rightarrow 0_1^+$ transition (shifted and unshifted) in the total projection of the $\gamma - \gamma$ matrix. The lifetime of the 2_1^+ state was determined from the normalized intensities of the shifted and unshifted peaks using the differential decay curve (DDC) method [36,37]. The variation of the normalized intensities with distance, the so-called decay curves, are shown in Fig. 4. A lifetime value for the 2_1^+ state is obtained from the decay

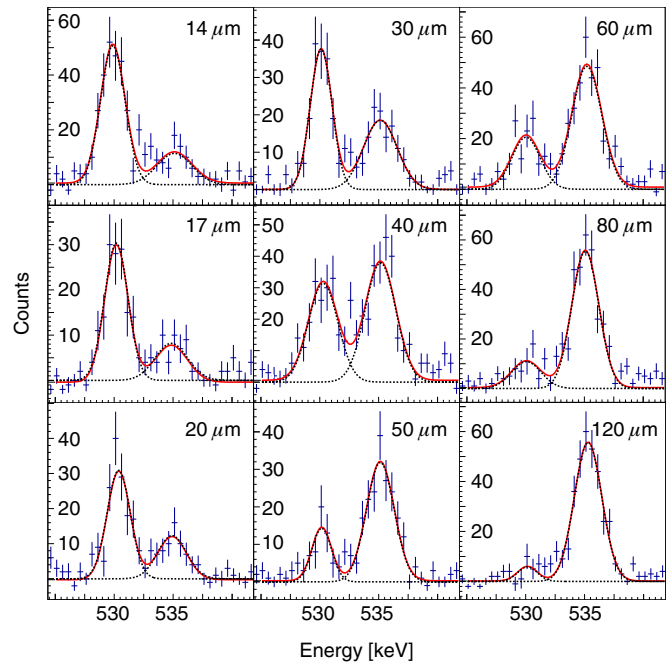

FIG. 3. (Color online) Background-subtracted spectra observed under forward angles showing the two components of the $2_1^+ \rightarrow 0_1^+$ transition after gating on the shifted component of the $4_1^+ \rightarrow 2_1^+$ transition for the nine different distances between the target and stopper foils.

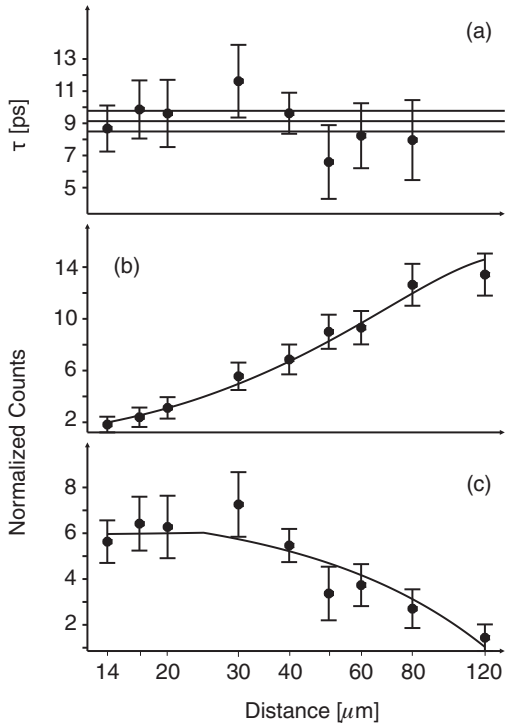

FIG. 4. Decay curves for the $2_1^+ \rightarrow 0_1^+$ transition showing the normalized intensities of the shifted (b) and unshifted (c) components of the transition as a function of distance. The resulting lifetimes for each distance and their mean value are shown in the top panel (a).

curves for each distance using the following expression:

$$\tau = \frac{1}{v}\frac{I^{us}}{\frac{d}{dx}I^{sh}}, \quad (1)$$

where I^{sh} and I^{us} are the normalized intensity of the shifted and unshifted components, respectively, and v is the recoil velocity. The results of the fitting procedure are included in Fig. 4. The intensity of the shifted component was fitted using two piecewise continuous polynomials of second order. The derivatives of these polynomials were fitted simultaneously to the decay curve of the unshifted component. The obtained lifetimes for each distance are shown in Fig. 4(a), from which a weighted mean value was determined. The lifetime of the 2_1^+ state was found to be 9.1(6) ps.

It was furthermore possible to gate on the shifted component of the $6_1^+ \rightarrow 4_1^+$ transition to select prompt feeding of the 4_1^+ state. However, the statistics is poor and only the two shortest distances show a significant variation in the relative intensities of the shifted and unshifted components of the $4_1^+ \rightarrow 2_1^+$ transition. It is evident that the lifetime of the 4_1^+ state is much shorter than that of the 2_1^+ state, but with only two data points in the sensitive region it was not possible to extract a reliable lifetime.

IV. DISCUSSION

The lifetime of $\tau = 9.1(6)$ ps measured for the 2_1^+ state in ^{140}Sm yields a reduced transition probability of $B(E2; 2_1^+ \rightarrow 0_1^+) = 0.216(15)\ e^2\mathrm{b}^2$, or 51(4) Weisskopf units. The $B(E2)$ value for ^{140}Sm is compared to those for other even-even Sm isotopes [29] in Fig. 5. This comparison of $B(E2)$ values illustrates how the collectivity of the 2^+ states increases rapidly with an increasing number of valence neutrons and neutron holes, respectively. The $B(E2)$ value obtained in the present measurement fits smoothly into the systematic trend.

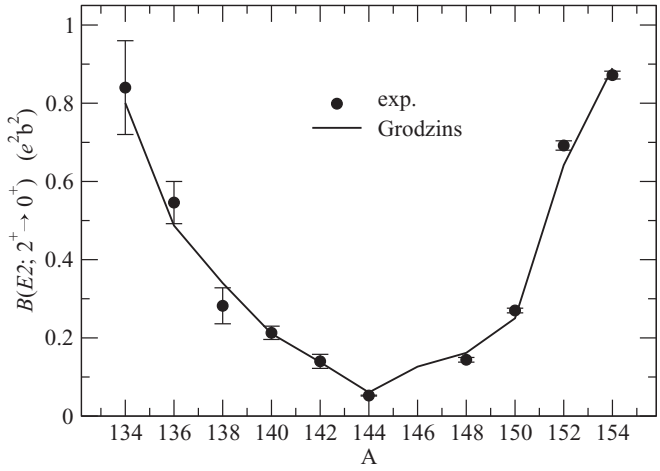

FIG. 5. Systematics of $B(E2; 2_1^+ \rightarrow 0_1^+)$ values for the even-even Sm isotopes. The data points show experimental values [29] including the one for ^{140}Sm measured in this work. The line shows $B(E2)$ values obtained from the energies of the 2_1^+ states by applying a modified Grodzins formula [39].

The $B(E2; 2_1^+ \rightarrow 0_1^+)$ value is in general correlated with the energy of the 2_1^+ state: With increasing collectivity, the $B(E2)$ values increase and the energies of the 2_1^+ states decrease. This correlation was first recognized by Grodzins [38] and is known as Grodzins rule. The original description of the correlation can be improved by introducing a term that depends on the neutron number relative to the most tightly bound nuclide within an isobaric chain [39]:

$$B(E2; 2_1^+ \rightarrow 0_1^+) = \frac{0.514Z^2}{E(2_1^+)A^{2/3}}[1.288 - 0.088(N - \bar{N})], \quad (2)$$

where $E(2_1^+)$ is given in keV and $B(E2; 2_1^+ \rightarrow 0_1^+)$ in $e^2\mathrm{b}^2$. The most stable neutron number $\bar{N}$ can be derived from the Weizsäcker mass formula as [39]

$$\bar{N} = \frac{A}{2}\frac{1.0070 + 0.0128A^{2/3}}{1 + 0.0064A^{2/3}}. \quad (3)$$

Figure 5 compares the experimental $B(E2; 2_1^+ \rightarrow 0_1^+)$ values with the values obtained from the modified Grodzins formula. The agreement is good and shows no indication of any anomalies for the chain of Sm isotopes on either side of the $N = 82$ shell closure. The $B(E2)$ value for ^{140}Sm obtained in this work fits very well into the systematic trend expected by the phenomenological modified Grodzins rule.

As can be seen in Fig. 5, the onset of collectivity below the $N = 82$ shell closure is almost as steep as for $N > 82$, although it does not show a sharp increase of the $B(E2)$ value as is observed from ^{150}Sm to ^{152}Sm. The latter has received much attention from both experimentalists and theorists. By

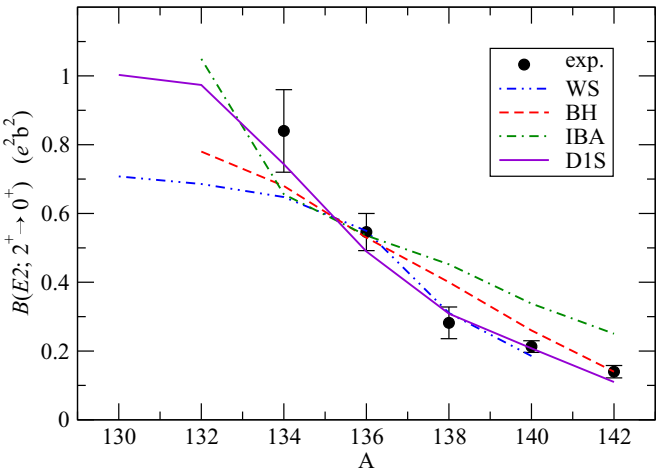

FIG. 6. (Color online) Experimental $B(E2; 2_1^+ \rightarrow 0_1^+)$ values for $^{134-138}$Sm [29], ^{140}Sm (present work), and the value for ^{142}Sm [40] compared to theoretical calculations using the general Bohr Hamiltonian (BH) based on a Nilsson potential [41], the interacting boson approximation (IBA) [19], a simple rotational model based on a deformed Woods-Saxon potential (WS) [14], and the 5DCH calculations based on the Gogny D1S interaction from the present work.

comparison, the onset of collectivity on the proton-rich side is less well studied and experimental data is more scarce.

Figure 6 compares the experimental $B(E2; 2_1^+ \rightarrow 0_1^+)$ values for the neutron-deficient even-even Sm isotopes to theoretical calculations. In addition to values that can be found in the literature, the figure shows results from new calculations, which were performed based on a mapped collective Hamiltonian in five quadrupole coordinates and the Gogny D1S interaction.

An early study of the neutron-deficient Sm isotopes includes Strutinsky calculations using a deformed Woods-Saxon potential, which find well-deformed prolate shapes for ^{134}Sm and ^{136}Sm and triaxial equilibrium shapes for the transitional nuclei ^{138}Sm and ^{140}Sm [14]. $B(E2; 2_1^+ \rightarrow 0_1^+)$ values were subsequently obtained using the rotational model and assuming a homogeneous charge distribution for the equilibrium deformation. However, in this work, only quadrupole and hexadecapole deformations were considered in the calculation of the $B(E2)$ values, whereas the triaxial degree of freedom was ignored. The resulting $B(E2)$ values are included in Fig. 6 and labeled WS. It is surprising to see that the $B(E2)$ values obtained in this way reproduce the experimental values for the transitional nuclei $^{136-140}$Sm correctly despite the inconsistency of neglecting triaxiality, whereas the further increase in the $B(E2)$ values for the more neutron-deficient isotopes, which are presumed to have axial symmetry, is not reproduced.

The curve labeled BH in Fig. 6 shows the results from a calculation using the Bohr Hamiltonian based on a Nilsson single-particle potential [41]. In this work, the collective potential was obtained by applying the Strutinsky microscopic-macroscopic method, and the moments of inertia were determined from the cranking model. The results predict a linear increase for the $B(E2)$ values with decreasing neutron number, whereas the experimental values show a steeper parabolic increase.

The evolution of collectivity in the neutron-deficient Sm isotopes was also the subject of a study employing the interacting boson approximation (IBA) [19]. The resulting $B(E2)$ values from the IBA-1 calculation, which makes no distinction between proton and neutron bosons, are included in Fig. 6. The IBA requires fitting of a set of parameters for each individual nuclide and the introduction of effective charges to calculate transition matrix elements. With a single effective boson charge fitted to reproduce the $B(E2; 2_1^+ \rightarrow 0_1^+)$ value for ^{136}Sm the IBA model cannot reproduce the relatively steep onset of collectivity for the Sm isotopes.

To better understand the onset of collectivity in the Sm isotopes below the $N = 82$ shell closure, the energies of the first 2^+ state and $B(E2; 2_1^+ \rightarrow 0_1^+)$ values were calculated using a microscopic structure model based on the constrained Hartree-Fock-Bogoliubov (CHFB) theory as well as a mapping to the five-dimensional collective Hamiltonian (5DCH) for quadrupole excitations at low energy [9]. The CHFB+5DCH calculations contain no free parameters except for those that specify the phenomenological D1S interaction [42,43]. Results of calculations for the Sm isotopic chain ranging from ^{130}Sm to ^{142}Sm are compared to experimental values in Table I and in Fig. 6. Table I also contains the average quadrupole deformation $\langle\beta\rangle$ and triaxiality parameter $\langle\gamma\rangle$ calculated for the ground state.

TABLE I. Comparison of experimental excitation energies of the 2_1^+ states and $B(E2; 2_1^+ \rightarrow 0_1^+)$ values for the even-even Sm isotopes below the $N = 82$ shell closure with five-dimensional configuration mixing calculations using the Gogny D1S interaction. The last two columns give the calculated mean quadrupole deformation parameters for the ground states.

	$E(2^+)$ (keV)		$B(E2; 2_1^+ \rightarrow 0_1^+)$ (e^2b^2)		$\langle\beta\rangle$	$\langle\gamma\rangle$
	expt	D1S	expt	D1S		
^{130}Sm	122	112	–	1.003	0.42	10°
^{132}Sm	131	119	–	0.974	0.40	10°
^{134}Sm	163	156	0.84(12)	0.743	0.35	15°
^{136}Sm	255	264	0.546(54)	0.489	0.28	22°
^{138}Sm	347	427	0.282(46)	0.309	0.21	27°
^{140}Sm	531	595	0.216(15)	0.208	0.17	29°
^{142}Sm	768	1218	0.140(18)	0.110	0.12	30°

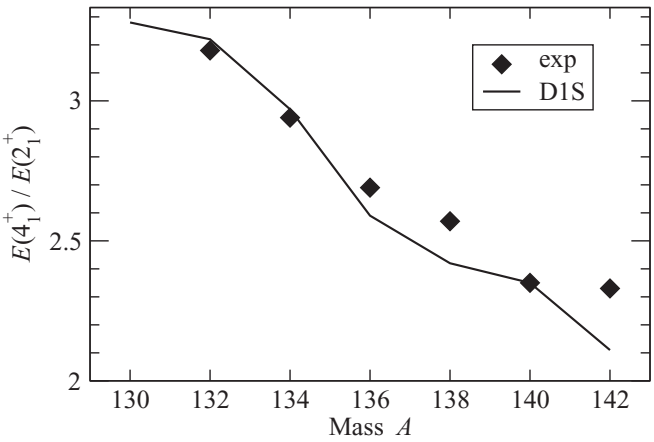

FIG. 7. Experimental excitation energy ratio $E(4_1^+)/E(2_1^+)$ compared to the values from the 5DCH calculations based on the Gogny D1S interaction from the present work.

The agreement between the 5DCH calculations with the D1S interaction and the experimental values is very good. The new calculations are the first to describe the steep onset of quadrupole collectivity in the neutron-deficient Sm isotopes correctly, with the calculated $B(E2)$ values reproducing the experimental values within their experimental uncertainties. The calculations predict that the increase in collectivity levels out below ^{132}Sm as the isotopic chain approaches neutron midshell. The calculated energies of the 2_1^+ states are very close to the experimental ones for the highly collective Sm isotopes with $N \leqslant 74$ up to ^{136}Sm. The calculated energies are somewhat too large for the heavier isotopes nearer to the shell closure. The agreement is still very reasonable, except for ^{142}Sm, for which the energy of the 2_1^+ state is overpredicted by 450 keV. It is, however, not surprising that a calculation that is based on a collective mean-field model fails to reproduce a state with single-particle character in a nucleus only two neutrons away from the shell closure.

The increase of the $B(E2; 2_1^+ \rightarrow 0_1^+)$ values with decreasing neutron number for the Sm isotopes below $N = 82$ is understood as being from a smooth transition of the nuclear shape. The collective character of the states in the ground-state band changes along with the nuclear shape. This is illustrated by the excitation energy ratio $R_{42} = E(4_1^+)/E(2_1^+)$, which is shown in Fig. 7 as a function of neutron number. The lightest Sm isotopes approach the rotational limit of $R_{42} = \frac{10}{3}$. The energy ratio decreases smoothly with neutron number and reaches $R_{42} = 2.35$ for ^{140}Sm and $R_{42} = 2.33$ for ^{142}Sm, much closer to the vibrational limit of $R_{42} = 2.0$. The 5DCH calculations are able to reproduce the energy ratios well. The shape transition is furthermore illustrated by the calculated average quadrupole deformation parameters for the ground states that are given in Table I. The lightest Sm nuclei ^{130}Sm and ^{132}Sm near neutron midshell are found to have a very large ground-state deformation of $\langle\beta\rangle = 0.42$ and $\langle\beta\rangle = 0.40$, respectively, with near axial symmetry. The overall deformation is found to decrease smoothly while the triaxial degree of freedom becomes more important as the $N = 82$ neutron shell closure is approached. The average quadrupole parameters for the ground state of ^{140}Sm are found to be $\langle\beta\rangle = 0.17$ and $\langle\gamma\rangle = 29^\circ$. According to the calculations, the large triaxial deformation found in ^{140}Sm is not rigid, but due to considerable γ softness. An experimental test of the γ-soft nature of the deformation in ^{140}Sm requires investigating higher-lying states beyond the 2_1^+ state, in particular nonyrast states. The Coulomb excitation data that were recently obtained [26,31] are expected to provide further information on the shape of ^{140}Sm and the onset of deformation in the neutron-deficient Sm isotopes.

V. SUMMARY AND CONCLUSIONS

The lifetime of the 2_1^+ state in ^{140}Sm was measured using the recoil distance Doppler shift method. Excited states in ^{140}Sm were populated in the reaction ^{124}Te(^{20}Ne,4n) at a projectile energy of 82 MeV, just above the Coulomb barrier. The distance between the target and a gold foil stopping the recoiling fusion-evaporation residues was adjusted with a plunger device, and γ rays were measured with the EAGLE array of HPGe detectors at the Heavy Ion Laboratory in Warsaw. Coincidence spectra were recorded for nine different distances ranging from 14 to 120 μm. The problem of delayed feeding was avoided by gating on the Doppler-shifted component of the $4_1^+ \rightarrow 2_1^+$ transition. The lifetime of the 2_1^+ state was found to be 9.1(6) ps, corresponding to $B(E2; 2_1^+ \rightarrow 0_1^+) = 0.216(15)\ e^2b^2$ or 51(4) Weisskopf units.

New microscopic structure calculations have been performed to further investigate the onset of quadrupole collectivity in the neutron-deficient Sm isotopes below the $N = 82$ shell closure. These five-dimensional collective Hamiltonian (5DCH) calculations based on the Gogny D1S interaction describe the evolution of $B(E2)$ values correctly and represent an improvement over previous calculations.

The results complete the systematics of $B(E2)$ values for neutron-deficient Sm isotopes below the $N = 82$ shell closure. The measurement of the lifetime of the 2_1^+ state is furthermore complementary to a recent Coulomb excitation experiment with radioactive ^{140}Sm beam [26,31] and can be used to constrain the Coulomb excitation analysis, improving the sensitivity to the spectroscopic quadrupole moment. Further insight into the evolution of nuclear shapes and collectivity can be expected to come from higher-lying yrast and nonyrast states and the electromagnetic matrix elements between them, which can be obtained from the Coulomb excitation data.

ACKNOWLEDGMENTS

This work was supported by the Research Council of Norway under project Grants No. 213442 and No. 205528, and by the National Science Center of Poland under Grant No. DEC-2013/10/M/ST2/00427. The authors acknowledge the support of GAMMAPOOL European Spectroscopy Resource for the loan of germanium detectors for the experimental campaign at HIL.

[1] R. Wadsworth *et al.*, Z. Phys. A **333**, 411 (1989).
[2] S. J. Zhu *et al.*, J. Phys. (London) G **21**, L57 (1995).
[3] R. F. Casten, D. D. Warner, D. S. Brenner, and R. L. Gill, Phys. Rev. Lett. **47**, 1433 (1981).
[4] F. Iachello, Phys. Rev. Lett. **87**, 052502 (2001).
[5] R. F. Casten and N. V. Zamfir, Phys. Rev. Lett. **87**, 052503 (2001).
[6] J. Meng *et al.*, Eur. Phys. J. A **25**, 23 (2005).
[7] R. R. Rodriguez-Guzman and P. Sarriguren, Phys. Rev. C **76**, 064303 (2007).
[8] L. M. Robledo, R. R. Rodriguez-Guzman, and P. Sarriguren, Phys. Rev. C **78**, 034314 (2008).
[9] J.-P. Delaroche, M. Girod, J. Libert, H. Goutte, S. Hilaire, S. Péru, N. Pillet, and G. F. Bertsch, Phys. Rev. C **81**, 014303 (2010).
[10] W. Urban *et al.*, Phys. Lett. B **258**, 293 (1991).
[11] W. Urban *et al.*, Phys. Lett. B **185**, 331 (1987).
[12] S. P. Bvumbi *et al.*, Phys. Rev. C **87**, 044333 (2013).
[13] P. E. Garrett *et al.*, Phys. Rev. Lett. **103**, 062501 (2009).
[14] B. D. Kern *et al.*, Phys. Rev. C **36**, 1514 (1987).
[15] A. Charvet *et al.*, Z. Phys. A **321**, 697 (1985).
[16] R. B. Firestone, J. Gilat, J. M. Nitschke, P. A. Wilmarth, and K. S. Vierinen , Phys. Rev. C **43**, 1066 (1991).
[17] T. Nikšić, P. Ring, D. Vretenar, Yuan Tian, and Zhong-yu Ma, Phys. Rev. C **81**, 054318 (2010).
[18] G. A. Lalazissis, M. M. Sharma, and P. Ring, Nucl. Phys. A **597**, 35 (1996).
[19] S. Pascu, N. V. Zamfir, Gh. Căta-Danil, and N. Mărginean, Phys. Rev. C **81**, 054321 (2010).
[20] D. Habs *et al.*, Z. Phys. A **250**, 179 (1972).
[21] W. Starzecki *et al.*, Phys. Lett. B **200**, 419 (1988).
[22] D. Bazzacco *et al.*, Phys. Lett. B **206**, 404 (1988).
[23] A. Berger, H.-E. Mahnke, H. Grawe, W. Semmler, and R. Sielemann, Z. Phys. A **321**, 403 (1985).
[24] S. Lunardi *et al.*, Phys. Rev. C **42**, 174 (1990).
[25] M. A. Cardona, S. Lunardi, D. Bazzacco, G. de Angelis, and V. Roca, Phys. Rev. C **44**, 891 (1991).
[26] M. Klintefjord *at al.*, Acta Phys. Pol. B **46**, 607 (2015).
[27] J. Samorajczyk *et al.* (unpublished).
[28] J. van Klinken *et al.*, KFK Report 1768 (KFK, Karlsruhe, 1973).
[29] S. Raman, C. W. Nestor, and P. Tikkanen, At. Data Nucl. Data Tables **78**, 1 (2001).
[30] A. Dewald, O. Möller, and P. Petkov, Prog. Part. Nucl. Phys. **67**, 786 (2012).
[31] M. Klintefjord *et al.* (unpublished).
[32] J. Ljungvall *et al.*, Phys. Rev. Lett. **100**, 102502 (2008).
[33] A. Gavron, Phys. Rev. C **21**, 230 (1980).
[34] J. Mierzejewski, A. A. Pasternak, M. Komorowska, J. Srebrny, E. Grodner, and M. Kowalczyk, [http://www.slcj.uw.edu.pl/compa].
[35] J. Mierzejewski *et al.*, Nucl. Instr. Meth. A **659**, 84 (2011).
[36] A. Dewald, S. Harissopulos, and P. von Brentano, Z. Phys. A **334**, 163 (1989).
[37] G. Böhm, A. Dewald, P. Petkov, and P. von Brentano, Nucl. Instr. Meth. A **329**, 248 (1993).
[38] L. Grodzins, Phys. Lett. **2**, 88 (1962).
[39] Th. Kröll *et al.*, Eur. Phys. J. Special Topics **150**, 127 (2007).
[40] R. Stegmann *et al.*, Phys. Rev. C **91**, 054326 (2015).
[41] L. Próchniak, K. Zajac, K. Pomorski, S. G. Rohozinski, and J. Srebrny, Nucl. Phys. A **648**, 181 (1999).
[42] J. Dechargé and D. Gogny, Phys. Rev.C **21**, 1568 (1980).
[43] J. Berger, M. Girod, and D. Gogny, Comput. Phys. Commun. **63**, 365 (1991).